ZnO indiffused MgO:PPLN ridge waveguides

LEWIS G. CARPENTER,[1,2,*] SAM A. BERRY,[1] REX H. S. BANNERMAN,[1] ALAN C. GRAY,[1] AND CORIN B. E. GAWITH[1,2]

[1]*Optoelectronics Research Centre, University of Southampton, Southampton, UK*
[2]*Covesion Ltd, Premier Way, Romsey, Hampshire, UK*
**lc906@orc.soton.ac.uk*

Abstract: We have demonstrated the first MgO:PPLN ridge waveguides based on ZnO indiffusion and dicing. The fabrication process utilizes ductile regime dicing of a planar waveguide layer producing Second Harmonic Generation (SHG) devices with a near-symmetric $sinc^2$ spectral profile, indicating highly uniform 40 mm long devices. A near circular pump mode is also obtained enabling efficient coupling to single mode telecommunication fibers. A conversion efficiency of 145%/W, for 1560-780 nm SHG, has been measured.

1. Introduction

Lithium niobate is widely used in frequency conversion because of its high $\chi^{(2)}$ optical nonlinearity [1] and ferroelectric crystal structure that allows domain engineering on the micron scale [2]. Periodically poled lithium niobate (PPLN) enables the ability to quasi-phase match $\chi^{(2)}$ processes throughout the 0.4-5.0 µm transparency range of the crystal [3,4]. Frequency conversion based on PPLN waveguides is typically more efficient than the bulk counterpart for cw operation, reducing device footprint and saving power on drive lasers/amplifiers [5]. PPLN waveguides offer a versatile means of generating tailored wavelengths for telecommunications [3,4], spectroscopy [5], single photon sources [6–8], state squeezing for quantum key distribution (QKD) [9], quantum communications [10,11], atom/ion trapping [12,13], and submarine communications [5].

PPLN waveguides have been investigated and manufactured via various routes and have been commercially available for a number of years. Mechanical bonding and thinning followed by dicing or etching of PPLN to form ridge and rib waveguides is a popular fabrication route [4,14,15] able to achieve conversion efficiencies of 4600%/W, albeit with an insertion loss of 4-5 dB at the 1550 nm pump wavelength [4,14]. Such bonding techniques typically require strict wafer cleanliness and total thickness variation (TTV) <5 µm [16]; deviations in waveguide dimensions of 150 nm have been shown to have significant impact on phase matching efficiency [15]. Annealed/reverse proton exchange (APE/RPE) enables channel waveguides with conversion efficiencies of ≥3500%/W, propagation loss ≤0.1 dB/cm and insertion loss of ≤0.4 dB [3]. APE/RPE waveguides suffer from photorefractive damage (PRD), which can be alleviated by operating the waveguide at 80-120 °C [3] but can in turn cause free proton migration and degradation of the waveguide [4]. APE/RPE waveguides also only support the TM mode, disqualifying them from Type-I/II operation which requires guidance for both orthogonal polarizations [4]. Titanium indiffused channel waveguides are common in lithium niobate and widely used in modulators for telecommunications. When used for frequency conversion to visible wavelengths, Ti indiffusion suffers significant PRD; even with a ridge geometry conversion efficiencies are still relatively low ~10%/W [17]. Indiffusion of Zn into LN has been shown to reduce PRD [18–23] and early planar waveguides were achieved via ZnO indiffusion into MgO doped LN by Young *et al.* [22,23]. In our own prior work on Zn-indiffused channel waveguides in PPLN, we achieved second

harmonic generation (SHG) conversion efficiencies of 59%/W with a propagation loss of 0.8 dB/cm at the 1550 nm pump wavelength [21].

In this paper, we combine planar ZnO indiffusion with ultra-precision dicing as a route towards easing the manufacturing tolerances of ridge waveguides in PPLN, whilst maintaining high conversion and coupling efficiencies in a thermally robust format capable of supporting both TE and TM polarizations. This is the first demonstration of a Zn indiffused MgO:PPLN ridge waveguide to be reported. Optimization of Zn indiffusion parameters by analyzing the modal output of planar waveguides is discussed, followed by spectral analysis of SHG towards optimized ridge dimensions. Phase matching conditions for varying pump powers versus SHG efficiency are also presented.

2. Waveguide fabrication

Fabrication of our ZnO indiffused MgO:PPLN ridge waveguides is performed in four stages as illustrated in Fig. 1.

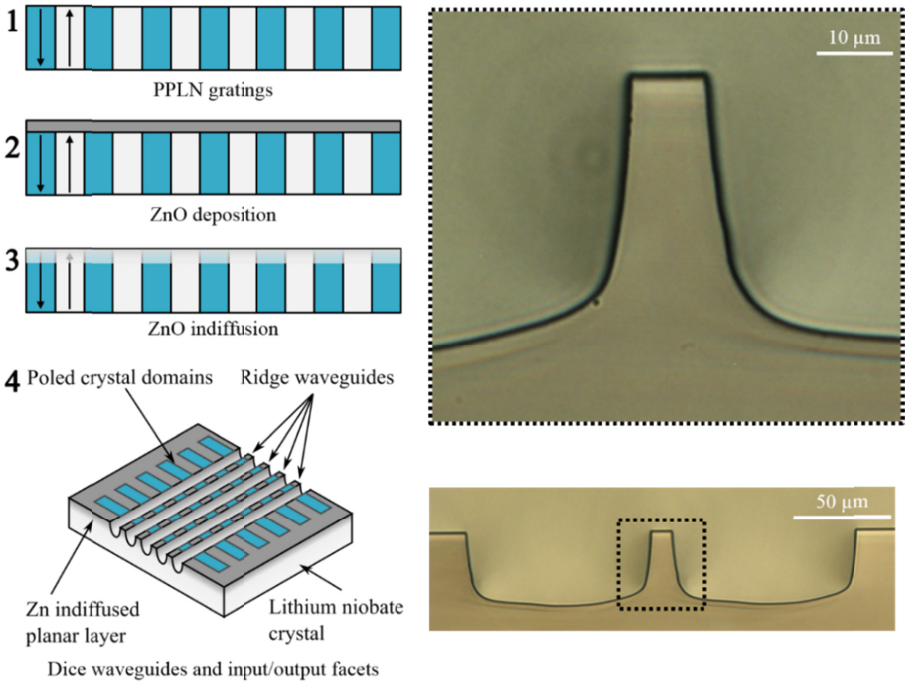

Fig. 1. ZnO indiffused MgO:PPLN ridge waveguide fabrication routine and diagram of a typical device. The microscopy shows images of a typical ridge waveguide facet.

Our ridge waveguide geometry was optimized for 1560-780 nm SHG by experimentally investigating how ZnO deposition thickness, indiffusion temperature and time, and ridge width affect SHG output intensity. Wafers of 5% Magnesium-doped Periodically-Poled Lithium Niobate (MgO:PPLN) were supplied by Covesion Ltd. Each wafer was 1 mm-thick and included multiple 1.2 mm-wide PPLN gratings with an 18.6 µm period, as suitable for 1560-780 nm SHG. We stimulate Type-0 SHG using the d_{33} coefficient, the most efficient nonlinear coefficient in lithium niobate, which require TM pump photons and generates TM second harmonic photons. After poling, standard solvent and acid cleaning was performed before deposition to remove particles and contamination prior to thin film deposition of ZnO via atomic layer deposition (Oxford Instruments Plasma Technology, FlexAL) to the + Z face of the crystal, the thickness of which was confirmed using an ellipsometer. Target ZnO thicknesses of 50 nm, 100 nm and 150 nm were deposited and ellipsometry measurements

(Woollam, Md2000D) verified the thicknesses at 42 nm, 121 nm and 150 nm (± 0.02 nm), respectively. Indiffusion was performed in a dedicated tube furnace with 1:1 ratio of oxygen/argon mixed atmosphere. Indiffusion parameters investigated were temperatures from 800 - 1000 °C with indiffusion times from 1 - 6 hours at peak temperature, each indiffusion used a 5 °C/min ramp rate. Surface metrology was collected via white light interferometry (ZeScope, ZeMetrics) after indiffusion to inspect the post-indiffusion surface roughnesses. It was found that surface roughnesses were generally 1-2 nm (Sa) for indiffusion times of 1 hour at temperatures of between 800 - 1000 °C for all ZnO thicknesses tested. For indiffusion times of 2-6 hours at 800 °C surface roughnesses increased to 12 nm (Sa). Thus, for this experiment the indiffusion time was kept constant at an hour and the indiffusion temperature and ZnO thicknesses were varied.

After indiffusion, the fundamental vertical mode second moment ($1/e^2$ for a Gaussian beam [24]) mode field diameter (MFD) of each planar layer was measured. A 1560 nm laser (Agilent, 81600B) was coupled into the planar waveguide via a cleaved single mode fiber and the resulting output light focused on to a InGaAs CCD camera (Raptor, Owl 640). The camera was moved to collect intensity profiles at recorded distances from the waveguide and results fitted to calculate the second moment MFD, as detailed in [24]. The calculated MFD for each recorded indiffusion temperature and ZnO thickness combination is plotted in Fig. 2, which shows that the smallest MFD is achieved with 150 nm of ZnO at 950 °C indiffusion temperature. As the ZnO thickness is reduced or the indiffusion temperature increased, the local Zn concentration is reduced and a well-confined mode is no longer supported; as the indiffusion temperature was reduced from 900 °C the modes produced were leaky hence the larger MFDs. Indiffusion at 800 °C did not produce waveguides.

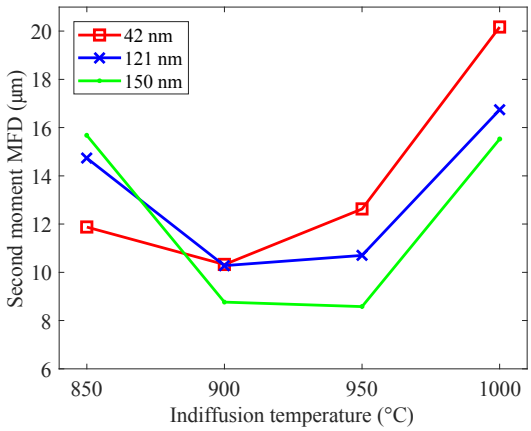

Fig. 2. Planar waveguide second moment MFD for varying indiffusion temperatures and ZnO thicknesses; the indiffusion dwell time for all waveguides was one hour once the peak processing temperature was reached. The minimum MFD is achieved with a 150 nm film of ZnO and for an indiffusion temperature of 950 °C.

Using the above parameters, further PPLN waveguides for 1560 nm SHG were fabricated via deposition of a nominal ZnO layer of 150 nm (measured at 170 nm) and indiffusion at 900 °C and 950 °C. After indiffusion, samples were diced into 40 mm by 10 mm chips with ridge waveguides and optical facets produced using similar machining parameters as described in [25]. Each chip was fabricated to include 10 ridge waveguides with widths that varied from 9.5 μm to 14 μm in 0.5 μm increments, each waveguide was cut parallel to the [100] X direction of the crystal with a 18.6 μm period PPLN. Note that these samples were not anti-reflection coated.

3. SHG characterization

SHG was measured and evaluated for each ridge width and indiffusion temperature. A tunable seed laser (Agilent, 81689A) was injected into a polarizing maintaining (PM) erbium doped fiber amplifier (EDFA) (Keyopsys, CEFA-C-PB-HP) after a polarizer. Light was coupled into the ridge waveguide using a collimator and aspheric lens (Thorlabs, ZC618APC-C and C560TME-C), by adjusting the focal length of the zoom collimator, coupling efficiency was optimized by monitoring SHG signal. All launch optics were antireflection coated at the pump wavelength. The pump polarization was optimized to launch TM light. Output light was collimated with an aspheric lens (Thorlabs, A375-B) and a dichroic filter (Thorlabs, DMLP-950) was used to separate the pump and the SHG wavelengths on to a thermal (Thorlabs, S302C) and silicon (Thorlabs, S121C) detector respectively.

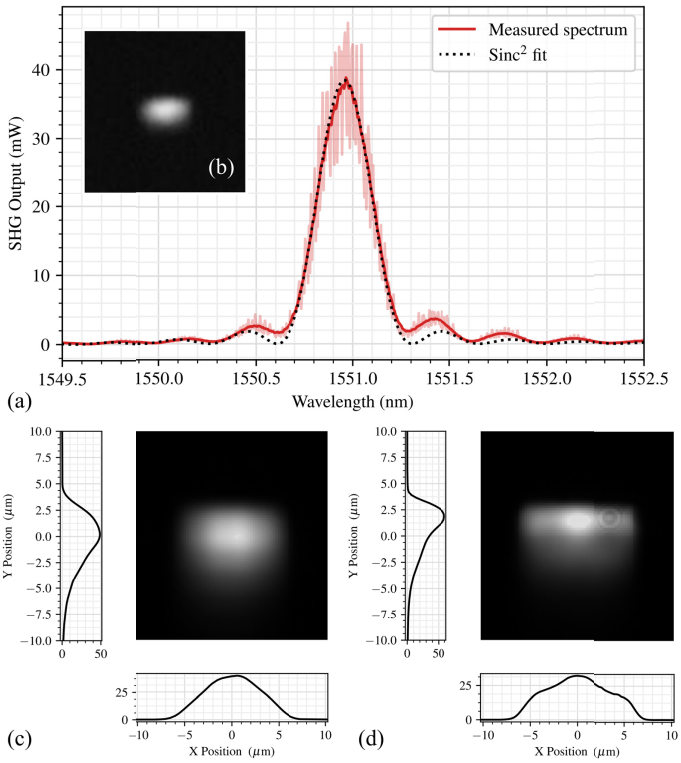

Fig. 3. SHG spectra and mode profiles for a ridge waveguide fabricated with a 170 nm layer of ZnO indiffused at 900 °C for 1 hour, a 13.4 μm diced ridge width, and 18.6 μm period PPLN grating. (a) SHG spectra, the red lines show experimental data along with an average fit and the black dotted line shows a theoretical fit for the waveguide. (b) SHG mode from nonlinear excitation. Output mode profiles from linear excitation for (c) pump and (d) SHG output wavelengths.

Figure 3(a) displays the SHG spectra for a ridge waveguide fabricated with a 170 nm layer of ZnO indiffused at 900 °C for 1 hour, a 13.4 μm diced ridge width, and 18.6 μm period PPLN grating. SHG spectra were measured using an incident pump power of 300 mW. As the effective refractive index is different for each ridge waveguide width, phase matching was achieved by varying the pump wavelength for each different ridge width at room temperature (~21 °C). Figure 3(a) shows the SHG output versus wavelength spectra for the highest efficiency waveguide measured. The apparent noise on the trace arises from Fabry-Pérot fringes (light solid red line) from the uncoated waveguide end facets with a free spectral range of ~14 pm aliased by the 5 pm sample rate. The solid red line indicates a rolling

average of device performance without the FP fringes. To investigate the quality of phase matching, which is directly related to the waveguide's uniformity and poling quality, a theoretical fit was added to the plot (black dotted line), which had a calculated r^2 of 0.957 (r^2 = coefficient of determination) with respect to the $sinc^2$ profile of the rolling averaged data. Other ridge widths and waveguides indiffused at 950 °C were either less efficient or had broadened SHG spectra some with multiple peaks. SHG spectral broadening comes from fabrication imperfections in the waveguides which manifest as an effective refractive index variation caused by non-uniform Zn indiffusion or ridge width variation along the length of the device [4,26]. The mode profiles of the waveguide are shown in Figs. 3(b), 3(c) and 3(d). Figure 3(b) shows the SHG mode, taken with a Si CCD, whilst phase matched. Figures 3(c) and 3(d) have been used to calculate a second moment MFD. A MFD for the pump was measured to be 10.8 and 10.0 µm in the x and y axes respectively, and 12.1 and 7.9 µm in the x and y axes for the SHG mode. Figure 3(b) was measured with an EDFA (AFL, BBS-1550A-TS) and Figs. 3(d) with a 780 nm SLED (Exalos, EX210060-01) where the multimode nature at the SHG wavelength can be seen. Insertion losses of ~1.1 dB and ~0.9 dB for pump light with a free space launch and glued fiber (Corning, PM 1550) v-groove, respectively have been achieved. This loss includes propagation loss, mode mismatch and Fresnel losses; insertion losses in comparable 5 cm long bonded and thinned PPLN waveguides have been reported at 5 dB [4].

3.1 Pump power sweep

Power scaling measurements for SHG and conversion efficiency were measured for various pump powers using the same optical setup used to collect SHG spectra. The pump laser power was varied from 0.15 – 2.23 W in 0.11 W steps with the waveguide at room temperature (~21 °C). Transmitted power was collected simultaneously for pump and SHG from the output facet of the waveguide, with results as shown in Fig. 4. The loss of pump power through output coupling optics was measured at −1.37 dB ± 0.02 dB across 1540-1565 nm EDFA band and is accounted for within the data in Fig. 4 by adding this offset to the measured pump.

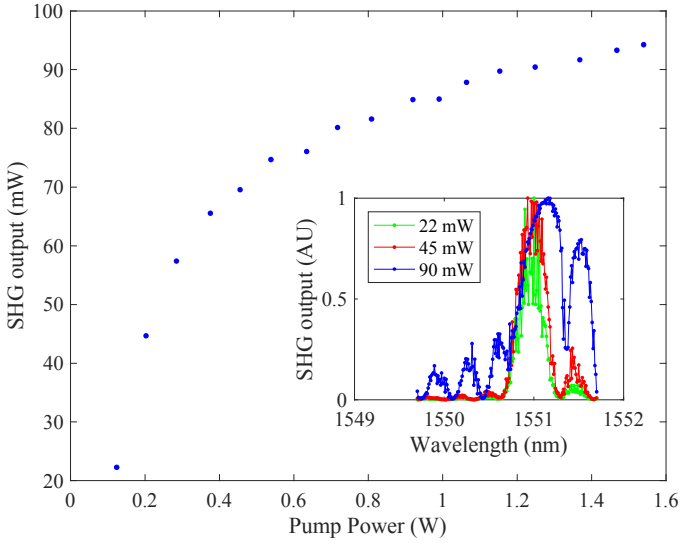

Fig. 4. SHG output and conversion efficiency for a ridge waveguide fabricated with a 170 nm layer of ZnO indiffused at 900 °C for 1 hour, a 13.4 µm diced ridge width, and 18.6 µm period PPLN grating. The highest measured efficiency was 145%/W, producing 22.3 mW of SHG with 124 mW of pump through the waveguide. The inset shows the phase matching spectra for different SHG output powers.

Figure 4 shows a maximum of 94.2 mW of second harmonic was produced. The highest conversion efficiency achieved was 145%/W producing 22.3 mW of SHG with 124 mW of pump being transmitted. There is a noticeable roll off in SHG at ~300 mW of pump power where parasitic nonlinearities and thermal effects become prevalent for increasing SHG power. The inset shown in Fig. 4 illustrates how the phase matching spectra becomes red detuned as pump power and SHG output is increased. The red detuning is evidence that SHG saturation is caused by dominate parasitic nonlinearities and thermal effects rather than PRD, which is shown to cause blue detuning of SHG phase matching spectra in titanium indiffused PPLN ridge waveguides [17]. In comparison to previous works in PPLN waveguides fabricated in a similar manner and pumping around 1550 nm the optical efficiency reported here is more than a factor of two higher. This is when compared to ridge waveguides fabricated by carbon ion implantation and dicing (60%/W) [26] and for our previous work with indiffused Zn channel waveguides (59%/W) [21]. Similar results have been presented for titanium indiffused PPLN waveguides where channel and ridge waveguides were compared, attributing increased efficiency to improved pump/SHG modal overlap and delayed roll off from PRD in the larger ridge geometry [17]. However, our efficiency is modest when compared to bonded and thinned waveguides [4,14] and APE/RPE waveguides [3]. Moreover, bonded and thinned waveguides, as mentioned earlier, rely on strict wafer cleanliness to ensure successful contact bonding [16]. Waveguide form variation must be minimized to the hundreds of nanometers level to ensure efficient devices, which is challenging to achieve when grinding and polishing planar waveguides [4,14,15]. Bonding and grinding both are not required in our ridge waveguide fabrication. APE/RPE waveguides suffer from free proton migration at elevated pump powers, which can degrade the waveguides [4]. This is partially a result of the low temperatures used in the proton exchange and subsequent annealing stages. By contrast our Zn indiffused ridge waveguides are thermally stable, because of their 900 °C ion based indiffusion, allowing operation at elevated pump powers and temperatures without waveguide degradation.

4. Conclusion

We have demonstrated a process for the manufacture of ridge waveguides in MgO:PPLN based on indiffusion of a ZnO planar layer followed by dicing of ridges in the ductile regime. Design parameters for 1560-780 nm SHG have been investigated, leading to devices with near-symmetric sinc^2 SHG output power vs wavelength spectral profile, indicating a uniform effective refractive index along the 40 mm length of the waveguides, and a near circular pump mode enabling efficient coupling to single mode telecommunication fibers. Mode size optimization has been used to maximize SHG output with the fabricated waveguides being single mode at the pump wavelength thus decreasing launch tolerances when compared to bonded and thinned PPLN waveguides [4], which are often multimode and require selective launching and careful spot size choice to maximize power launched into the fundamental spatial mode. Overall optical-to-optical conversion efficiencies of 145%/W have been measured, with a SHG output of ~22 mW for 124 mW of pump power, representing an improvement over alternative ridge waveguide manufacturing methods when measured in similar operating regime [14,26]. Indiffusion of ZnO into PPLN has previously been shown to improve resistance to photorefractive and future investigations at 780-390 nm SHG will be performed to confirm if this persists in our ridge format at these challenging wavelengths.

Funding

Innovate UK (KTP009534-A01); Engineering and Physical Sciences Research Council (EP/P034160/1, EP/R041636/1); Royal Academy of Engineering.

Acknowledgments

The authors would also like to thank Dr Harold Chong and Dr Katrina Morgan for technical support on ALD and ellipsometry.

References

1. P. F. Bordui and M. M. Fejer, "Inorganic crystals for nonlinear optical frequency conversion," Annu. Rev. Mater. Sci. **23**(1), 321–379 (1993).
2. M. Yamada, N. Nada, M. Saitoh, and K. Watanabe, "First-order quasi-phase matched LiNbO3 waveguide periodically poled by applying an external field for efficient blue second-harmonic generation," Appl. Phys. Lett. **62**(5), 435–436 (1993).
3. C. Langrock, S. Kumar, J. E. McGeehan, A. E. Willner, and M. M. Fejer, "All-optical signal processing using $\chi(2)$ nonlinearities in guided-wave devices," J. Lit. Technol. **24**(7), 2579–2592 (2006).
4. T. Umeki, O. Tadanaga, and M. Asobe, "Highly efficient wavelength converter using direct-bonded PPZnLN ridge waveguide," IEEE J. Quantum Electron. **46**(8), 1206–1213 (2010).
5. W. P. Risk, T. R. Gosnell, and A. V. Nurmikko, *Compact Blue-Green Lasers* (Cambridge University, 2003), Chap 1–2.
6. S. Arahira, N. Namekata, T. Kishimoto, H. Yaegashi, and S. Inoue, "Generation of polarization entangled photon pairs at telecommunication wavelength using cascaded $\chi 2$ processes in a periodically poled LiNbO3 ridge waveguide," Opt. Express **19**(17), 16032–16043 (2011).
7. T. Meany, L. A. Ngah, M. J. Collins, A. S. Clark, R. J. Williams, B. J. Eggleton, M. J. Steel, M. J. Withford, O. Alibart, and S. Tanzilli, "Hybrid photonic circuit for multiplexed heralded single photons," Laser Photonics Rev. **8**(3), 42–46 (2014).
8. P. R. Sharapova, K. H. Luo, H. Herrmann, M. Reichelt, T. Meier, and C. Silberhorn, "Toolbox for the design of LiNbO3-based passive and active integrated quantum circuits," New J. Phys. **19**(12), 123009 (2017).
9. F. Kaiser, B. Fedrici, A. Zavatta, V. D'Auria, and S. Tanzilli, "A fully guided-wave squeezing experiment for fiber quantum networks," Optica **3**(4), 362–365 (2016).
10. S. Tanzilli, W. Tittel, H. De Riedmatten, H. Zbinden, P. Baldi, M. De Micheli, D. B. Ostrowsky, and N. Gisin, "PPLN waveguide for quantum communication," Eur. Phys. J. D **18**(2), 155–160 (2002).
11. L. Oesterling, F. Monteiro, S. Krupa, D. Nippa, R. Wolterman, D. Hayford, E. Stinaff, B. Sanguinetti, H. Zbinden, and R. Thew, "Development of photon pair sources using periodically poled lithium niobate waveguide technology and fiber optic components," J. Mod. Opt. **62**(20), 1722–1731 (2015).
12. T. Lévèque, L. Antoni-Micollier, B. Faure, and J. Berthon, "A laser setup for rubidium cooling dedicated to space applications," Appl. Phys. B **116**(4), 997–1004 (2014).
13. D. Akamatsu, M. Yasuda, T. Kohno, A. Onae, and F. L. Hong, "A compact light source at 461 nm using a periodically poled LiNbO3 waveguide for strontium magneto-optical trapping," Opt. Express **19**(3), 2046–2051 (2011).
14. R. Kou, S. Kurimura, K. Kikuchi, A. Terasaki, H. Nakajima, K. Kondou, and J. Ichikawa, "High-gain, wide-dynamic-range parametric interaction in Mg-doped LiNbO3 quasi-phase-matched adhered ridge waveguide," Opt. Express **19**(12), 11867–11872 (2011).
15. M. Chauvet, F. Henrot, F. Bassignot, F. Devaux, L. Gauthier-Manuel, V. Pêcheur, H. Maillotte, and B. Dahmani, "High efficiency frequency doubling in fully diced LiNbO3 ridge waveguides on silicon," J. Opt. **18**(085503), (2016).
16. D. Tulli, D. Janner, and V. Pruneri, "Room temperature direct bonding of LiNbO3 crystal layers and its application to high-voltage optical sensing," J. Micromech. Microeng. **21**(085025), (2011).
17. S. Pal, B. K. Das, and W. Sohler, "Photorefractive damage resistance in Ti:PPLN waveguides with ridge geometry," Appl. Phys. B **120**(4), 737–749 (2015).
18. W. Tsai, T. Chiang, L. Liu, P. Chang, and Y. Su, "Time and temperature dependent study of Zn and Ni codiffused LiNbO3 waveguides," J. Lit. Technol. **33**(23), 4950–4956 (2015).
19. E. Cantelar, J. A. Sanz-García, G. Lifante, F. Cussó, and P. L. Pernas, "Single polarized Tm3+ laser in Zn-diffused LiNbO3 channel waveguides," J. Appl. Phys. **86**(161119), (2005).
20. R. Twu, C. Huang, and W. Wang, "Zn indiffusion waveguide polarizer on a Y-cut LiNbO3 at 1.32-μm wavelength," IEEE Photonics Technol. Lett. **12**(2), 161–163 (2000).
21. L. Ming, C. Gawith, K. Gallo, M. O'Connor, G. Emmerson, and P. Smith, "High conversion efficiency single-pass second harmonic generation in a zinc-diffused periodically poled lithium niobate waveguide," Opt. Express **13**(13), 4862–4868 (2005).
22. W. M. Young, R. S. Feigelson, M. M. Fejer, M. J. F. Digonnet, and H. J. Shaw, "Photorefractive-damage-resistant Zn-diffused waveguides in MgO:LiNbO(3)," Opt. Lett. **16**(13), 995–997 (1991).
23. W. M. Young, M. M. Fejer, M. J. F. Digonnet, A. F. Marshall, and R. S. Feigelson, "Fabrication, characterization and index profile modeling of high-damage resistance Zn-diffused waveguides in congruent and MgO:lithium niobate," J. Lit. Technol. **10**(9), 1238–1246 (1992).
24. BS EN ISO 11146–1:2005, Lasers and laser-related equipment. Test methods for laser beam widths, divergence angles and beam propagation ratios. Stigmatic and simple astigmatic beams (British Standard, 2005)

25. L. G. Carpenter, S. A. Berry, and C. B. E. Gawith, “Ductile dicing of LiNbO3 ridge waveguide facets to achieve 0.29 nm surface roughness in single process step,” Electron. Lett. **53**(25), 1672–1674 (2017).
26. L. Wang, C. E. Haunhorst, M. F. Volk, F. Chen, and D. Kip, “Quasi-phase-matched frequency conversion in ridge waveguides fabricated by ion implantation and diamond dicing of MgO:LiNbO(3) crystals,” Opt. Express **23**(23), 30188–30194 (2015).